

# PCCP

Physical Chemistry Chemical Physics

Accepted Manuscript

This article can be cited before page numbers have been issued, to do this please use: E. Alloa, V. Grande, R. Dilmurat, D. Beljonne, F. Wuerthner and S. C. Hayes, *Phys. Chem. Chem. Phys.*, 2019, DOI: 10.1039/C9CP01874C.



This is an Accepted Manuscript, which has been through the Royal Society of Chemistry peer review process and has been accepted for publication.

Accepted Manuscripts are published online shortly after acceptance, before technical editing, formatting and proof reading. Using this free service, authors can make their results available to the community, in citable form, before we publish the edited article. We will replace this Accepted Manuscript with the edited and formatted Advance Article as soon as it is available.

You can find more information about Accepted Manuscripts in the [Information for Authors](#).

Please note that technical editing may introduce minor changes to the text and/or graphics, which may alter content. The journal's standard [Terms & Conditions](#) and the [Ethical guidelines](#) still apply. In no event shall the Royal Society of Chemistry be held responsible for any errors or omissions in this Accepted Manuscript or any consequences arising from the use of any information it contains.

## ARTICLE

## Resonance Raman study of the J-type aggregation process of a water soluble perylene bisimide

Elisa Alloa,<sup>a</sup> Vincenzo Grande,<sup>b</sup> Rishat Dilmurat,<sup>c</sup> David Beljonne,<sup>c</sup> Frank Würthner,<sup>b</sup> and Sophia C. Hayes<sup>a,\*</sup>

Received 00th January 20xx,  
Accepted 00th January 20xx

DOI: 10.1039/x0xx00000x

Perylene bisimides (PBIs) are dyes known for combining high absorption and emission in the visible region with their thermal and photochemical stability. H-bond-directed aggregation driven by free imide groups has been reported to promote the uncommon J-type aggregate formation of PBIs. J-aggregates are highly desired thanks to their bathochromically shifted narrow absorption and fluorescence due to excitonic coupling, together with hyperchromicity and superradiance compared to the monomer. Herein we present the water soluble **MEG-PBI** showing interesting aggregation in water and in solid state. Unlike its hydrophobic counterparts, **MEG-PBI** aggregates in water upon increasing temperature, indicating an entropy-driven self-assembly. Temperature-dependent Resonance Raman (RR) spectroscopy was employed for the structural characterization of **MEG-PBI** in aqueous solution versus toluene and in aggregated thin films, employing excitation at different wavelengths to probe the contribution of various chromophores to the supramolecular structure of the aggregate. We find that the perylene core distorts upon aggregation, where the bonds along the perylene long N-N axis lengthen and the ones perpendicular to that shorten, suggesting a head-to-tail arrangement due to H-bonding between neighboring units.

### Introduction

Organic optoelectronics is an area of research that has seen substantial growth during the past decade, thanks to the success of devices such as organic light-emitting diodes (OLEDs), organic field effect transistors (OFETs), and organic photovoltaics (OPVs). New developments<sup>1,2</sup> in the field have been achieved by moving from small molecules and polymers with desirable electronic properties to electronically active  $\pi$ -conjugated molecules capable of self-assembly through non-covalent forces, such as hydrogen bonding, electrostatic forces, metal–ligand, dipole–dipole, hydrophobic,  $\pi$ – $\pi$  interactions, and steric repulsion. Even inspiration from the biological world had an influence in the field: similarly to light harvesting systems in photosynthetic antenna complexes, in supramolecular assemblies the excitation is coherently transferred by resonant emission and absorption phenomena from one molecule to a neighboring one, i.e. dye molecules play directly the role of transferring units.<sup>3</sup> These excitons can extend over ordered and coupled molecular units in the solid state, where the packing arrangement of the aggregates

governs the favored optical outcome for the chosen technological application.<sup>4</sup> Supramolecular assemblies deliver a strong impact on opto-electronics as they offer the chance to create structures that incorporate directed molecular order, with significant dynamics through bond reversibility.<sup>5</sup> To develop organic semiconductor technologies, it is necessary to understand the complex structural arrangements and processes present in the materials and how these can affect device performance. Spectroscopic methods can provide insights in the supramolecular assembly, utilizing external stimuli such as temperature to tune the desired spectral state of the chemical system.<sup>6,7,8</sup>

Within this research field, J-aggregates constitute a particularly interesting class of materials, especially in organic photonics due to the fact that self-assembly of molecules into a head-to-tail arrangement results in coherent  $\pi$ -electron states that are delocalized over part of the molecular aggregate.<sup>9</sup> Perylene tetracarboxylic acid bisimides, in short perylene bisimides (PBI) are a highly interesting class of dyes for J-aggregates, with very promising functional properties, which were recently exploited in all-polymer photonic microcavities.<sup>10</sup> PBIs have been well recognized as versatile chromophores with strong absorption, near unity fluorescence quantum yield, and high thermal and photochemical stability.<sup>11</sup> Their high chemical flexibility allows various substitutions thereby tuning reactivity and spectral properties.<sup>12</sup> Due to these appealing assets, perylene bisimides and their related derivatives have continuously received significant attention for their potential applications in biomedicine (bioimaging)<sup>13</sup> and molecular optoelectronic devices, such as organic photovoltaics (e.g. as acceptors),<sup>14,15</sup>

<sup>a</sup> University of Cyprus, Department of Chemistry, P.O. Box 20537, 1678, Nicosia, Cyprus. E-mail: shayes@ucy.ac.cy

<sup>b</sup> Universität Würzburg, Institut für Organische Chemie und Center for Nanosystems Chemistry, Würzburg, 97074, Germany.

<sup>c</sup> Laboratory for Chemistry of Novel Materials, University of Mons, 20 Place du Parc, B-7000 Mons, Belgium.

Electronic Supplementary Information (ESI) available: RR, IR and computational details. See DOI: 10.1039/x0xx00000x

field-effect transistors,<sup>16</sup> light-emitting diodes,<sup>17</sup> light-harvesting arrays<sup>18</sup> and LCD color filters.<sup>19</sup> Furthermore, the elaboration of water-soluble PBI-based aggregate systems via self-assembly evolved as a promising research avenue because of its possible exploitation in biological systems. In the most recent research of some of us, PBI J-aggregates could be formed by hydrogen-bonded self-assembly in water, which was quite surprising if we consider that water is a very competitive solvent for the self-complementary hydrogen bonding between the imide units of the PBIs.<sup>20</sup> Interestingly, however, these hydrogen-bonded self-assembled nanofibers with J-type coupling and fluorescence properties only occurred at elevated temperature, obviously driven by entropy from the less ordered PBI room temperature hydrogel material. This chemical system has been named "aquamaterial"<sup>21,22</sup> because of its capability to behave as a hydrogel-like material with unique and useful properties: the red-to-blue color transition appears indeed to be exploitable in the development of cutting-edge applications e.g. as photonic material in microcavities or as lyotropic liquid crystals. Its unique properties primarily derive from its large extended  $\pi$ -systems, together with its various supramolecular aggregate-based architectures.<sup>23</sup> H-bonded aggregation driven by self-complementary free-imide groups has also been reported to promote alternative J-type aggregate formation in non-polar solvents.<sup>24</sup> Thanks to non-covalent connectivity, such PBIs form very sophisticated supramolecular fibers, enabling interesting photophysics involving exciton coherence and migration.<sup>25</sup> More specifically, hydrogen-bond donors/acceptors and  $\pi$ - $\pi$  interaction were employed for the design of these functional PBI chromophores with such unique spectroscopic properties: these forces collaborate in a self-complementary way to build a supramolecular connection among the monomers in order to achieve a wired structure with a face-to-face arrangement, typical of a mixed J/H aggregate.<sup>26</sup> Double/triple-stranded aggregates are thus formed by elongating  $\pi$ - $\pi$  stacked units, where their building blocks are aligned with a translational offset.<sup>15,27</sup> The water-soluble PBI previously reported by some of us, depending on the excitonic coupling extent, forms an amorphous aggregate structure with a monomer-like UV/Vis spectrum at room temperature, where the units exhibit a co-facial arrangement with weak H-type coupling, or a slipped packing with J-type coupling when the temperature increases, with fluorescence in the far-red.<sup>20</sup>

In this work, the transition from an amorphous monomer-like state to an ordered J-aggregated state (and vice versa) was investigated through spectroscopic methods, in order to better understand the driving forces and mechanisms of aggregation of these promising supramolecular architectures. Resonance Raman (RR) spectroscopy was used to elucidate the structure of the PBI monomers in the assembly. Various supramolecular assemblies have been studied with this vibrational technique, especially in the biological field, where e.g. supramolecular amyloid fibrils could be spectroscopically detected by UVRR, as

well as structural changes due to pH-induced chirality changes in their supramolecular structure.<sup>28,29</sup> In this field, RR was also employed in detecting structural alterations in photosynthetic antenna complexes of green bacteria,<sup>30</sup> or in the design and testing of new anti-malaria drugs by sensing structural information on porphyrin moieties in hemes.<sup>31</sup> Different self-organized systems widely employed in supramolecular chemistry such as porphyrins<sup>32,33,34</sup> or carotenoids<sup>35</sup> have also been structurally monitored by RR. Moreover, RR spectroscopy has been adopted in the field of biosensors to accurately measure the strength of host-guest complexations.<sup>36,37</sup> Even though RR has been utilized for the characterization of a plethora of supramolecular systems, PBIs have only been analyzed by Raman spectroscopy as individual molecules<sup>38,39</sup> and not in their J aggregated state. This spectroscopic method is very powerful especially due to the selectivity to a particular chromophore: by tuning the excitation wavelength to the absorption band of a particular chromophore in a chemical system, chromophore-related vibrations only are substantially enhanced. Therefore, evolution in the structure of a molecule monitored by changes in key vibrational bands during the supramolecular assembly process can give mechanistic details difficult to obtain easily with other methods.

The present study focuses on a PBI molecule designed to self-assemble via hydrogen bonding and  $\pi$ - $\pi$  interactions into a supramolecular J-aggregated structure. This dye bears amphiphilic bay substituents consisting of twelve glycol chain residues at meta-positions of a tetraphenoxy-functionalized perylene bisimide, enabling water solubility. RR spectroscopy was employed here to investigate in detail the ground state conformation of this perylene bisimide (PBI) system. In order to provide a complete insight in the structure and the role of hydrogen bonding in the self-assembly, the selectivity of resonance Raman was exploited to elucidate the contribution of specific chromophores through excitation in the UV and visible spectral region. Our results indicate that the supramolecular structure of the PBI studied undergoes a change in its aggregation pattern, showing an elongation along the main fiber axis at higher temperatures, resulting in a J-aggregated nanofiber, confirming the involvement of hydrogen bonding.

## Experimental and computational methods

### Materials

The water soluble **MEG-PBI**, a meta-ethyleneglycol-functionalized tetraphenoxy perylene bisimide bearing four dendrons decorated with methoxy-triethyleneglycol chains, is presented in Fig. 1.<sup>20</sup> **MEG-PBI** is a dark-blue solid that gradually dissolves in water under stirring. **MEG-PBI** water / deuterated water solutions were prepared at a concentration of 62.5  $\mu\text{M}$ , while a further comparative experiment was performed with a 6-times diluted solution (10  $\mu\text{M}$ ). Higher concentrations were necessary to initiate the aggregate formation in toluene, with a

minimum concentration of 2.9 mM. A thin film with **MEG-PBI** in the aggregated state, was prepared by spin-coating a 1mM **MEG-PBI** in  $\text{CHCl}_3$  solution on quartz films.

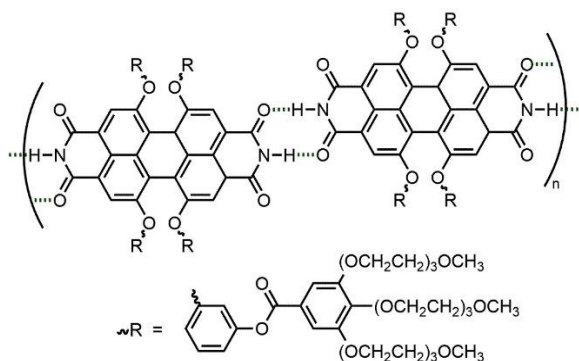


**Fig. 1** Structure of the water-soluble perylene bisimide. J-aggregates are formed upon hydrogen bonding of the imide N-H of one molecule to the C=O of a neighboring one. Bottom: The side chains "R" attached to the main PBI core.

### Resonance Raman Spectroscopy

The aqueous **MEG-PBI** samples were excited at 217 nm, 282 nm, 266 nm and 532 nm, of which the former two were obtained from Raman-shifting in  $\text{H}_2$  gas the second harmonic of an Nd:YAG laser at 532 nm, while the 266 nm wavelength is generated from the fourth harmonic of the laser (PRO 230-30 Hz, Spectra Physics). Further excitations were provided at 405 and 473 nm by CW diode lasers (Monopower<sup>TM</sup> 405-50-MM, Alphas, and Ultralasers, 473 nm, 50 mW OEM DPSS Laser). The aqueous solutions were placed in a custom-made cryocell (Fig. 2) that was fitted to the cold finger of a sample-in-vacuum closed-cycle cryostat (CCS-150, JANIS). The sample cavity had a 13 mm diameter and 3 mm pathlength. The cryostat was fitted on a translation stage for periodic translation of the sample during data acquisition in order to avoid degradation. The toluene samples were placed in a 0.2 mm pathlength suprasil cuvette (Hellma) with a 12.5  $\mu\text{l}$  sample volume. Experiments in the UV were performed with the sample in a spinning cell consisting of an EPR suprasil tube (diameter: 4 mm) attached to a rheostat-controlled motor for choice of rotation speed.



**Fig. 2** Aqueous **MEG-PBI** solutions at RT (left) and 313 K (right).

Use of the spinning cell prolonged the lifetime of the samples. Both the cuvette and the tube were placed inside a thermostated holder (thermal mantle) controlled by a water bath. In addition, modest excitation powers (0.1 mW for the pulsed lasers, 1 mW, for CW lasers) were employed to avoid decomposition of the sample. The Raman scattered light was

collected in a  $135^\circ$  backscattering geometry and delivered to a 0.75 m focal-length Czerny–Turner spectrograph, equipped with a 1200-grooves/mm UV-enhanced holographic grating. Experiments in the UV utilized the 2400 gr/mm UV-enhanced holographic grating. The slit width was set to 100  $\mu\text{m}$  providing for  $\sim 5 \text{ cm}^{-1}$  spectral resolution for the visible wavelengths used in this work, and up to  $\sim 12 \text{ cm}^{-1}$  for the experiments in the UV. The scattered light was detected by a LN<sub>2</sub>-cooled 2048×512 pixel, back-illuminated UV-enhanced CCD detector (Spec10:2KBUV/LN, Princeton Instruments). Each spectrum presented here is the accumulation of 6 to 12 10-min spectra. Raman spectra of aqueous **MEG-PBI** samples were obtained at room temperature and 313 K. A long incubation period (overnight) was necessary to reach a stable aggregate state of **MEG-PBI**. A color change from violet (at room temperature) to blue (at 313 K) confirmed the transition from one form to the other, as shown in Fig. 2. In the case of toluene samples, experiments were run at 283 K, room temperature and 333 K and the temperature was allowed to stabilize for 10 - 15 min. In this case, the sample turned from dark blue (at 283 K) to violet (at 333K). Moreover, the absorption spectrum was monitored before and after each experiment in order to check for conformational changes and sample degradation. Frequency calibration of the spectra was accomplished with the use of cyclohexane. MATLAB and ORIGIN were used for spectral treatment and analysis.

### Computational methods

Structural optimization of **MEG-PBI** was carried out on its methylated precursor obtained by replacing the twelve glycol chain units with methoxy groups. The structural optimization was performed with Density Functional Theory (DFT) calculations at the B3LYP/6-31+G\*\* level of theory utilizing the Gaussian16<sup>40</sup> program package. All the calculations were carried out in the gas phase. Calculated IR and Raman spectra, as well as the electronic properties and HOMO–LUMO energies, were obtained at the same level of theory. For simplicity, absorption wavelengths and oscillator strengths were calculated on the **MEG-PBI** precursor, obtained after removing the tris-(methoxytriethyleneglycol) gallate units. The calculations were carried out using time-dependent DFT (TD-DFT) with the B3LYP functional and the 6-31(d,p) basis set,<sup>41,42</sup> based on the optimized structure in the gas phase. The structures were rendered with the UCSF Chimera package. Chimera is developed by the Resource for Biocomputing, Visualization, and Informatics at the University of California, San Francisco (supported by NIGMS P41-GM103311).<sup>43</sup> The nature of the electronic excitations was explored by extracting natural transition orbitals<sup>44</sup> (NTO) from the Gaussian16 check point files using the Multiwfn software.<sup>45</sup>

### Results and discussion



The temperature-dependent optical response of **MEG-PBI** is presented in Fig. 3. The absorption spectra for **MEG-PBI** in water at RT and 313 K correspond to the monomer-like amorphous state and the J-type supramolecular assembly, respectively, with the latter showing a large bathochromic shift from 563 nm for the 0-0 peak to 633 nm, as usually observed for J-aggregates.

Temperature-dependent Resonance Raman (RR) spectroscopy was employed for the structural characterization of PBI in these two different molecular states. A range of excitation wavelengths were chosen as indicated in the figure in order to observe the involvement of various chromophores in the supramolecular assembly. Excitation in the visible range corresponds to absorption due to the perylene core (according to the DFT computational study, see ESI, Figure S1 and Table S1), while excitation in the UV probes the phenyl rings and the bisimide groups on the PBI.<sup>24</sup> Monitoring any spectral changes

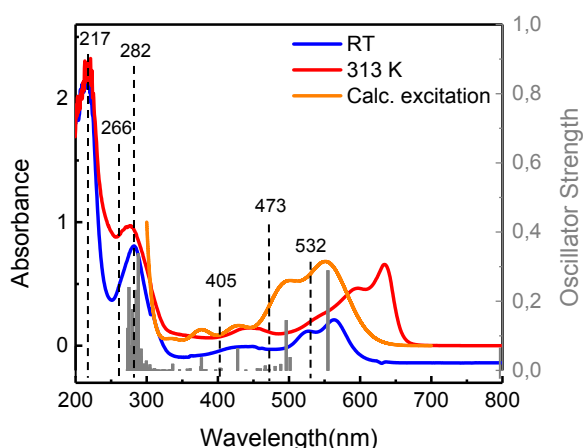


**Fig. 3** UV-vis spectrum of **MEG-PBI** in aqueous solution as a function of temperature. TD-DFT calculated transitions are shown in vertical grey lines, with the right scale indicating their oscillator strength. The overall calculated spectrum is shown in orange, while the black dotted lines indicate the excitation wavelengths used for the resonance Raman measurements.

on resonance with the side-chains can provide insights in their participation in the aggregation process, while on resonance with the perylene core structure and its associated bisimide, one can assess the extent of hydrogen bonding and its impact on the core structure. The bisimide group skeleton resembles the structure found in nucleobases (thymine and uracil) that absorb in the UV with bands around 210 nm and 260 nm that can be assigned to  $\pi$ - $\pi^*$  transitions.<sup>46,47</sup> Excitations at 217, 266 and 282 nm probe phenyl rings both in the perylene core and in its side chains, however, in variable proportion.

#### Visible resonance Raman

The normalized RR spectra of the **MEG-PBI** amorphous and aggregate phase in aqueous solution and in thin films acquired at 532 nm are presented in Fig. 4. Even though similar spectra

are observed for the two states, distinct differences are observed that provide some insight on the structure of the aggregate. Specifically, a 5  $\text{cm}^{-1}$  downshift is observed for the 1355  $\text{cm}^{-1}$  and 1555  $\text{cm}^{-1}$  bands upon aggregation, while the bands at 1395  $\text{cm}^{-1}$  and 1600  $\text{cm}^{-1}$  show a 5  $\text{cm}^{-1}$  upshift. The band at 1447  $\text{cm}^{-1}$  remains unchanged at the two different

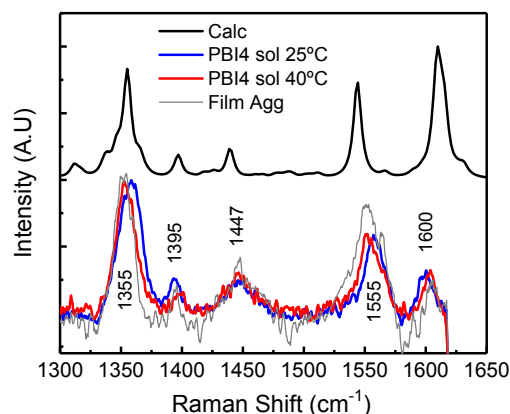


**Fig. 4** Top: Calculated Raman spectrum of **MEG-PBI** in vacuum (scale factor \*0.97). Bottom: Resonance Raman spectra of **MEG-PBI** in aqueous solution at RT (monomer-like) and 313 K (aggregate) and in a thin film with excitation at 532 nm.

temperatures. RR spectra of **MEG-PBI** aggregates in thin films are in full agreement with the spectrum displayed by **MEG-PBI** aggregates in solution.

Computation of the normal modes of **MEG-PBI** provided insights on the structure of the aggregate through correlation of the varied vibrational fingerprint upon aggregation to specific structural changes (Fig. 5 and Table 1). The experimental spectrum of the amorphous state is well reproduced by the computation, which considers the molecule in vacuum, with the observed bands corresponding to vibrational modes of the perylene core. The bands at 1355  $\text{cm}^{-1}$  and 1555  $\text{cm}^{-1}$  are assigned to C=C stretching along the long axis of the perylene (the N-N axis, see Fig. 5), while the bands at 1395  $\text{cm}^{-1}$  and 1600  $\text{cm}^{-1}$  are associated with C=C stretching perpendicular to the N

**Table 1** Experimental and Calculated Raman Frequencies ( $\text{cm}^{-1}$ ).

EXP ( $\lambda_{\text{exc}} = 532 \text{ nm}$ )		CALC (vacuum)		Assignment of PBI core vibrations†
Monomer-like	J-Aggr			
1359	1352	1383		$\nu_{\text{C=C}} \parallel$ to N-N axis
1395	1398	1423		ip $\delta_{\text{C-H}} / \nu_{\text{C=C}} \perp$ to N-N axis
1447	1447	1467		s $\nu_{\text{C=C}}$ (central ring)
1557	1550	1575		$\nu_{\text{C=C}} \parallel$ N-N axis
1598	1603	1641		ip $\delta_{\text{C-H}} / \nu_{\text{C=C}} \perp$ to N-N axis
1706	1706	1791		$\nu_{\text{C=O}}$ (free C=O)

†v: stretch,  $\delta$ : bend, ip: in-plane, s: symmetric, ||: parallel,  $\perp$ : perpendicular and broadening of the 1447  $\text{cm}^{-1}$  peak for the amorphous phase  
DOI: 10.1039/C9CP01874C

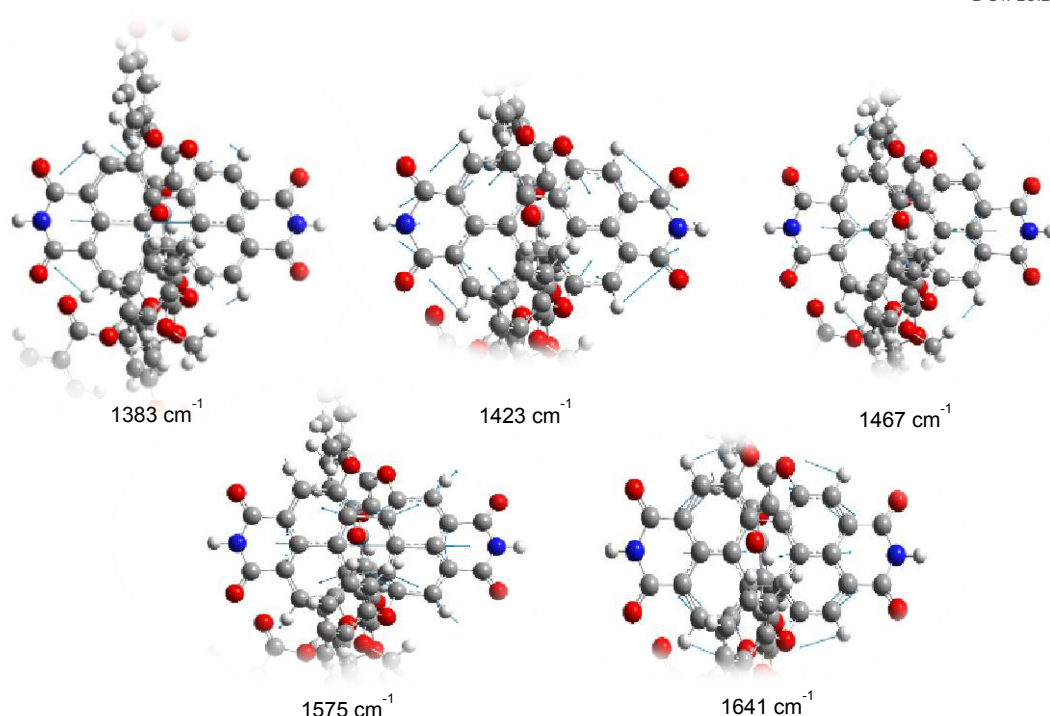
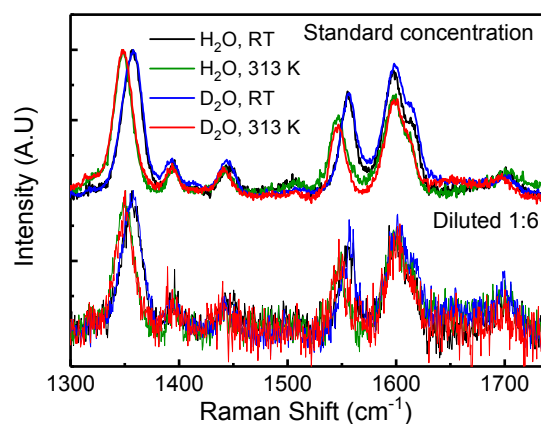


Fig. 5 Calculated vibrational normal modes for MEG-PBI. The blue arrows denote the displacement vectors.

- N axis and along the periphery of the core in combination with in-plane C-H bending. The band at 1447  $\text{cm}^{-1}$  corresponds to C=C stretching involving the central aromatic ring, where the perylene is twisted. Based on this evidence, a distortion of the perylene core upon aggregation can be proposed, where the bonds along the perylene long axis lengthen and the ones perpendicular to that shorten, with elongation parallel to the N-N axis, likely induced by hydrogen bonding of the imide protons with carbonyls from neighboring molecules, resulting in a head-to-tail arrangement (Fig. 1). Overlap of the N-H stretch with the strong O-H stretching bands of water in the high frequency region made direct observation of hydrogen bonding effects difficult.

In order to assess whether the chosen concentration affects the aggregation process and whether an entirely monomeric conformation could be possible with a less close packing of the units, the temperature-dependent experiment was performed with a 1:6 diluted sample (10  $\mu\text{M}$ ) with excitation at 473 nm, again on resonance with the main core of the PBI, where most of the shifts appear due to the elongation of the aggregated supramolecular structure. As Fig. 6 clearly shows, even though the spectra are noisier due to a lower signal, the same modes and shifts appear at both concentrations, suggesting that we are dealing with the same conformer as in the 62.5  $\mu\text{M}$  concentrated sample and that a monomer-like conformation can be hypothesized even for the concentrated solution at low temperature. A difference in the relative intensities for the 1555 and 1600  $\text{cm}^{-1}$  modes, along with a slight shift to higher energies

at both concentrations, suggests that the nature of this electronic transition differs from that at 532 nm. This observation is in agreement with the finding from the DFT calculations that a second strong electronic transition involving the perylene core exists close to this excitation wavelength (calculated at 494 nm, Figure S1). The experiment was also performed in deuterated water, in order to interrogate the role of the imide N-H proton in the aggregation process<sup>48</sup>, which is directly involved in H-bonding to the carbonyl groups of another PBI. The signal resembles the spectra obtained in water, confirming that the vibrations observed are due to C=C stretches in the core, without involvement of the imidic N-H. A 5  $\text{cm}^{-1}$  downshift is observed for the 1700  $\text{cm}^{-1}$  peak at high-temperature in the deuterated sample (J-aggregated



**Fig. 6** RR spectra of **MEG-PBI** as a function of concentration and temperature with excitation at 473 nm. The comparison is between the standard solution concentration (62.5  $\mu\text{M}$ ) and a 1:6 diluted one. RR spectra are also shown for **MEG-PBI** in deuterated water.

conformation). As shown below, this vibration is associated with the carbonyl bond not involved in H-bonding in the aggregate. In deuterated water, free C=Os of aggregated samples that can hydrogen bond to the solvent vibrate at lower energies, similarly to the case of the C=O band of deoxyribonucleotide d-CMP and d-GMP, with 266 and 218 nm excitation, that downshifts upon deuteration.<sup>49</sup>

The lower frequency region was also investigated with RR spectroscopy in order to monitor the presence of 'out of plane' modes, widely reported in literature as fingerprint of J-aggregation according to the theory of Aggregation-Enhanced Raman Scattering (AERS).<sup>50</sup> An intense peak at 254  $\text{cm}^{-1}$  is indeed observed in the aggregated state only (Fig. 7) in both solution and film, which corresponds to the out-plane core vibration calculated at 234  $\text{cm}^{-1}$ . It is noted in the literature that the significant enhancement of low-frequency modes occurs only when the excitation wavelength is on resonance with the J-aggregate absorption band of the molecule. Moreover, according to the AERS theory, the enhanced peak seen in the low frequency region may be due to  $\pi$ - $\pi$  stacking among units in the fibers, which is consistent with the supramolecular assembly of **MEG-PBI** molecules.<sup>51</sup>

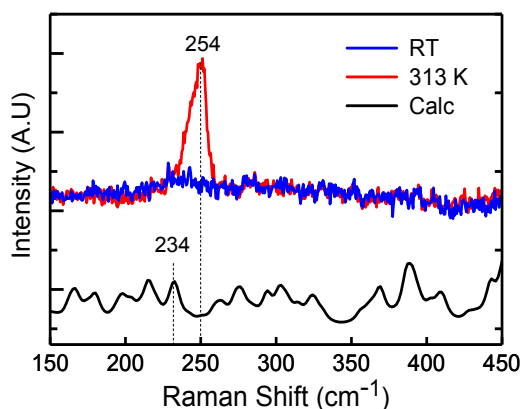


**Fig. 7** Top: Experimental Resonance Raman spectra of **MEG-PBI** in water solution with excitation at 473 nm showing the amorphous (blue) and J-aggregate (red) conformation. Bottom: Calculated Raman spectrum of **MEG-PBI** in vacuum.

#### UV Resonance Raman

The hydrophobic effect plays a major role in the self-assembly process of **MEG-PBI** in water and monitoring N-H bonding of the perylene core imide as well as interactions among the side chains of the supramolecular structure is fundamental. Exploring further excitation wavelengths can help attain this goal. From Fig. 8, showing RR spectra with excitation chosen on resonance with different chromophores in the molecule, it is immediately evident that the peaks in all graphs closely match

the calculated Raman spectrum, thus the simulation can provide a good tool for interpretation of results. It is apparent that different modes are enhanced when the excitation is changed from the visible to the UV, facilitating thus the elucidation of the nature of the different electronic transitions. Specifically, observing the fingerprint region from 1300 to 1700  $\text{cm}^{-1}$ , one can see that the 1600  $\text{cm}^{-1}$  mode is the most prominent band in the UVRR spectra compared to the 1355  $\text{cm}^{-1}$  band in the visible. Moreover, the other peaks show reduced intensity and some disappear, which is a clear sign that the resonance with the main core is reduced in the UV. There is also a perceptible shift in the bands in the visible versus the UVRR spectra (highlighted with dotted lines in Fig. 8); this is an indication that different chromophores are probed. Another clear evidence is the presence of a peak at 1729  $\text{cm}^{-1}$ , which, according to the calculations and FT-IR spectra (see below), corresponds to the carbonyl bonds in the esters of the side chains of the molecule. For a detailed description of the observed bands and assignments to the calculated modes see Table S2.

Excitation in the UV is used here to enhance the scattering from the imide groups, where the hydrogen bond between PBI units is suggested to develop, in order to directly probe any interactions upon aggregation due to the sensitivity of amide vibrations to hydrogen bonding. Different N-H vibrations can be

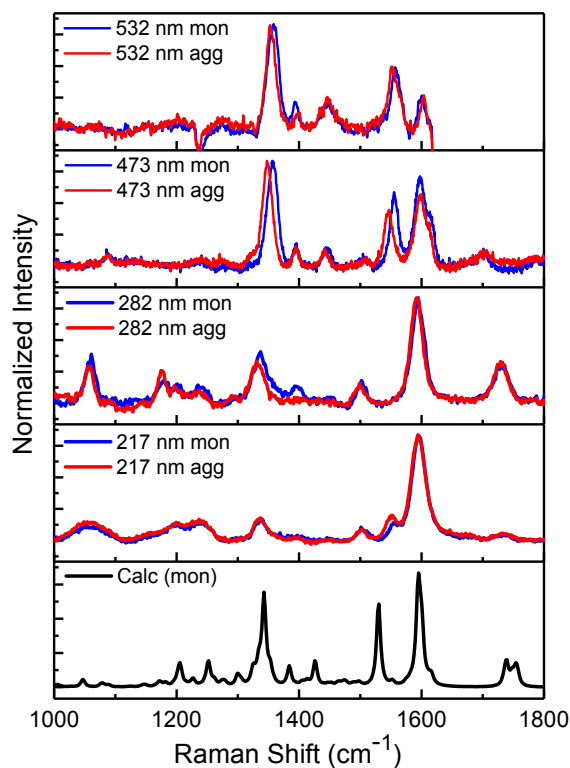


**Fig. 8** Wavelength-dependent RR spectra of **MEG-PBI** in water showing the monomer-like (at room temperature) and the J-aggregate (at 313 K). Bottom: Calculated Raman spectrum of **MEG-PBI** in vacuum. Dotted lines highlight major band shifts between visible and UV spectra.

examined that provide a signature in the Raman spectrum, as has been shown extensively in the literature on proteins and DNA.<sup>49,52–55</sup> In particular, resonance Raman studies on nucleotides resembling the PBI imide group (uracil, thymine) at different excitations in the UV show the sensitivity of N-H vibrations to their local environment.<sup>49</sup> Besides amides, UV excitation is highly resonant with aromatic rings,<sup>56</sup> therefore the involvement of the aromatic side chains can be resolved. Excitation of aqueous **MEG-PBI** at 217 nm (Fig. 8) reveals an intense band that corresponds to the C=C phenyl vibrations from the side-chains and smaller bands that correspond to either ring vibrations from the core or the side chains (see Table S1). A noticeable difference with aggregation is observed in the 1555 cm<sup>-1</sup> band that corresponds to a C=C stretch along N-N axis due to the interaction among the PBI units, as it has been established for the visible excitations. It is possible that the bisimide moiety absorbs at this wavelength, therefore the experiment was repeated in deuterated water (Fig. S2) in order to see changes associated with N-D substitution, the crucial connecting point among units in the aggregation process. However, no drastic changes are observed in the spectra that could be associated with the N-D bending vibrations. This suggests that excitation at 217 nm is associated entirely with absorption of the aromatic rings in the molecule. Thus, the invariability of the RR spectra at this wavelength suggests that the aromatic side chains are not involved in the supramolecular assembly.

At 282 nm excitation, the most significant change observed in the RR spectra involves the 1395 cm<sup>-1</sup> band that disappears upon self-assembly. This corresponds, according to the calculations, to N-H bending of the imide. Disappearance of this band is consistent with highly restricted movement due to the self-assembly. Assignment of this band to N-H bending was confirmed by repeating the experiment in deuterated water. Fig. 9 shows that the peak disappears upon deuteration, as the

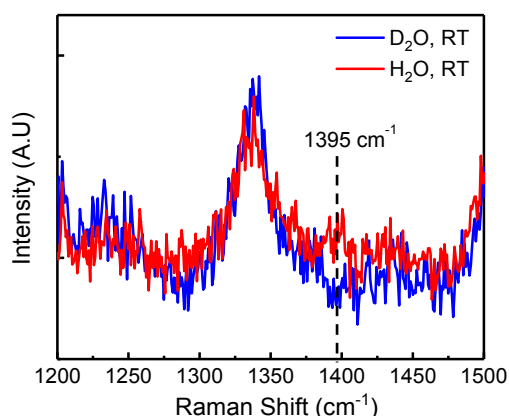


**Fig. 9** RR spectra of **MEG-PBI** in water and deuterated water with excitation at 266 nm at room temperature. The dotted line indicates the position of the N-H bend band.

N-D bending band is downshifted with respect to the N-H bend. Isotopic substitution has been a valuable tool for band assignment, where for example in proteins N-D substitution clearly shifts the amide II band that involves out-of-phase N-H bending from  $\approx 1555$  to  $\approx 1450$  cm<sup>-1</sup>.<sup>57</sup> In addition, a shift is observed for the 1331 cm<sup>-1</sup> peak with temperature, which could be ascribed to the main ring elongation that we see in the visible (see Table S1). TD-DFT calculations of the excitation spectrum of **MEG-PBI** confirm the involvement of the imide moiety in this UV transition (see ESI, Table S1).

The PBI aggregated structure in water was compared to the case in an organic solvent, specifically toluene, to obtain further information about the formation of the supramolecular structure, and in particular to understand certain vibrational signatures in the water samples. In organic solvents, PBIs aggregate at lower temperatures (283 K) and dissociate upon increasing temperature (333 K) where the molecule reaches a full monomeric state. The absorption spectra of the molecule in toluene as a function of temperature (Fig. 10) are significantly different to the ones in water (Fig. 3) both in shape and peak position in the two phases. The intensity ratio of the

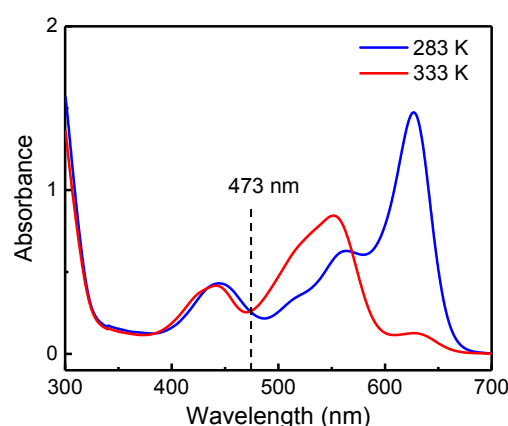


**Fig. 10** Absorption spectra of **MEG-PBI** toluene solution at 283 K (aggregate) and 333 K (monomer). The excitation wavelength chosen is in an isosbestic point.

0-0 and 0-1 vibronic bands increases noticeably at low temperature as expected for J-aggregates, while both spectra are slightly shifted to higher energies in toluene compared to water. Resonance Raman spectra were obtained with excitation at 473 nm in resonance with the PBI core. The spectra in Fig. 11 show similar relative intensities and shifts in water and in toluene for each phase (amorphous and aggregate). In particular, the conformations in both solvents share the same peak shift direction; however, the shift is smaller in toluene (4 cm<sup>-1</sup>), which suggests a weaker hydrogen bond between the units. Moreover, a more intense band is observed at 1704 cm<sup>-1</sup> in the monomer state, corresponding to the free imide carbonyl, and a weak band at  $\sim 1670$  cm<sup>-1</sup> associated with the hydrogen-bonded carbonyl in the aggregate. While a distortion



of the perylene core emerges from the band shifts in the aggregate as suggested above for water, increased intensity of the free imide C=O band in toluene reveals a molecule with reduced structural stiffening. In water instead a supramolecular structure is preserved even in the monomer form, where the units are distant in space from each other, resembling single units but still ordered in a macrostructure and hydrogen-bonded to surrounding water molecules, which can be identified, according to previous work,<sup>58</sup> as a less ordered H-aggregate structure. A change in relative intensity is clear for the carbonyl peak ( $1704\text{ cm}^{-1}$ ) and for the  $1555\text{ cm}^{-1}$  band (ring

vibration along the main perylene axis): more specifically, both these monomer bands show in toluene a strong increase with increasing temperature. A progressive reduction of stiffness from aggregate to a fully monomeric conformation can be

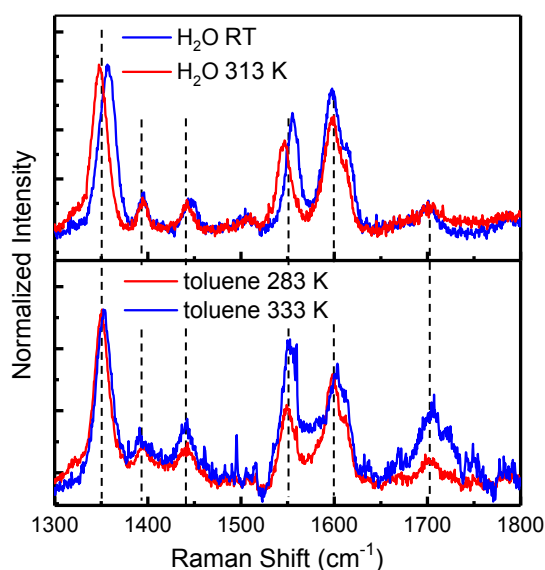


**Fig. 11** RR spectra of MEG-PBI in water versus toluene with excitation at 473 nm. The selected temperatures allow for the corresponding monomer and aggregate species in each solvent: (red) aggregate, (blue) monomer.

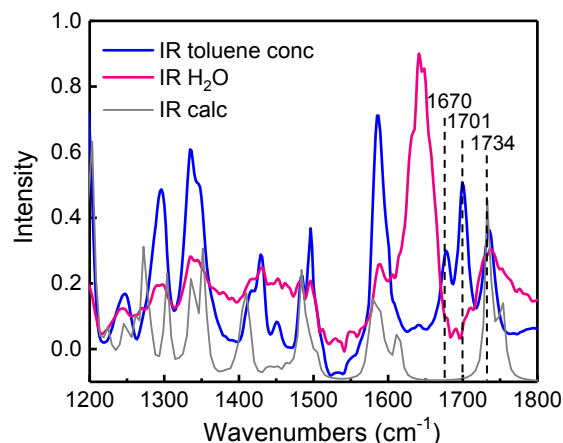


**Fig. 12** FT-IR spectra of toluene and water solution of **MEG-PBI** run at room temperature, compared with IR calculation (in vacuum, scale factor \*0.97). The strong band  $\sim 1650\text{ cm}^{-1}$  in the IR spectrum of **MEG-PBI** in water corresponds to the bending mode of water.

identified and this evolution appears clearly in Fig. S3 in the changing intensity of these peaks with increasing temperature. The increased relative intensity of the  $1555\text{ cm}^{-1}$  band in the monomer, however, is reminiscent of the relative intensities observed in the water samples with excitation at 532 nm and can thus be associated with resonance with a similar transition, considering that the **MEG-PBI** absorption bands are blue shifted in toluene.

Driven by the intention of getting more insights in the carbonyl area, and specifically on the imidic C=O bond, complementary FT-IR was employed in order to provide further information on the aggregation process of **MEG-PBI** in water and toluene. Temperature dependent FT-IR measurements were previously performed on the solid material,<sup>20</sup> where three bands appeared in the C=O stretching region in the case of the aggregate:  $1678$ ,  $1700$ , and  $1735\text{ cm}^{-1}$ , corresponding to H-bonded imide carbonyls, free imide carbonyls and ester carbonyls in the side chains, respectively, in agreement with the Raman spectra described above (see Fig. 12). In the monomer state, the  $1678\text{ cm}^{-1}$  band disappears, as no H bonding exists with the imide proton of other units. FT-IR experiments in solutions of **MEG-PBI** in water and toluene were performed at RT, at which water hosts the monomer-like and toluene the aggregate component (Fig. 12). Good agreement is observed for the overall IR spectra in the two solvents, as well as with the calculated IR spectrum, with the exception of the position of the carbonyl bands that are sensitive to the solvent environment (the calculation was performed in vacuum); therefore the bands that appear in water correspond to real PBI bands, even if the **MEG-PBI** concentration is quite low and the solvent could interfere with

the analysis generating artifacts. As expected, some of the bands appear with similar frequency as in the Raman spectra but with different intensity. The  $1734\text{ cm}^{-1}$  peak appears in both solvents, due to the carbonyl group in the side chain esters. Two peaks at  $1670$  and  $1701\text{ cm}^{-1}$  are observed in toluene, confirming the previous FT-IR on the solid. Differently, for the amorphous phase in water only a small shoulder to the main ester band is observed in the position expected for the free carbonyl. However, the water bending band at  $1650\text{ cm}^{-1}$  is quite large and may possibly interfere with this band upon subtraction. Table S2 summarizes all the assignments of the Raman and IR bands according to the DFT calculations.

## Conclusions

In this work we have used vibrational spectroscopy to analyze the **MEG-PBI** structure upon transition from the monomer-like to the supramolecular J-aggregate phase. RR excitation energy variation facilitated selective probing of different chromophores in order to elucidate their participation in the aggregation process. FT-IR provided complementary insights to RR and could better discriminate the C=O signal involved in the hydrogen bonding among the PBI units. Temperature dependent RR spectroscopy revealed that upon aggregation the perylene core assumes a distorted conformation with elongation parallel to the N-N axis induced by hydrogen bonding of the imide protons with carbonyls from neighboring molecules resulting in a head-to-tail arrangement. A concentration-dependent analysis provided evidence that the sample concentration does not affect the aggregation pattern in the range studied. Moreover, a full agreement was found between the Raman spectrum displayed by the **MEG-PBI** aggregate in solution and that in thin film, suggesting that processing of the material from solution to solid does not affect its conformation. Deuteration of **MEG-PBI** helped identify the N-H bending vibration, which appeared only in the case of the monomer-like phase, as in the J-aggregate the constriction of the supramolecular structure causes a reduced intensity. As previously known, the aggregation pattern of **MEG-PBI** in water is influenced by the hydrophobic effect, as aggregation is an entropically-driven process. Our study revealed that in water a stiffer macrostructure is induced even in the monomer-like amorphous state, while monomers in toluene appear less tightly bound in the supramolecular structure. This difference in the PBI structure in the two J aggregates could affect the excitonic coupling between the monomer units and be responsible for the difference in the optical response observed in the two cases. Overall, this study provided key insights in the structure of this supramolecular system that can improve the understanding of the photophysical properties of this and other similar systems.

## Conflicts of interest

There are no conflicts to declare.

View Article Online  
DOI: 10.1039/C9CP01874C

## Acknowledgements

We acknowledge financial support from the EU Horizon 2020 Research and Innovation Programme, SYNCHRONICS Project (Grand Agreement 643238). EA and SCH would like to thank Dr. Pinakoulaki for access to the FTIR instrument. The work in Mons was supported by the European Union's Horizon 2020 Research and Innovation Program under the Marie Skłodowska-Curie Grant Agreement No. 722651 (SEPOMO project). Computational resources were provided by the Consortium des Équipements de Calcul Intensif (CÉCI), funded by the Fonds de la Recherche Scientifiques de Belgique (F.R.S.-FNRS) under Grant No. 2.5020.11, as well as the Tier-1 supercomputer of the Fédération Wallonie-Bruxelles, infrastructure funded by the Walloon Region under Grant Agreement No. 1117545. D.B. is a FNRS Research Director.

## Notes and references

- G. M. Whitesides and M. Boncheva, *Proc. Natl. Acad. Sci. U. S. A.*, 2002, **99**, 4769–74.
- B. Olenyuk, J. A. Whiteford, A. Fechtenkötter and P. J. Stang, *Nature*, 1999, **398**, 796–799.
- S. K. Saikin, A. Eisfeld, S. Valleau and A. Aspuru-Guzik, *Nanophotonics*, 2013, **2**, 21–38.
- A. V. Sorokin, *Funct. Mater.*, 2017, **24**, 005–392.
- A. Jain and S. J. George, *Mater. Today*, 2015, **18**, 206–214.
- F. Würthner, T. E. Kaiser and C. R. Saha-Moller, *Angew Chem Int Ed Engl*, 2011, **50**, 3376–3410.
- T. Kobayashi, in *World Scientific*, 1996, pp. 67–94.
- D. Embriaco, D. B. Balagurov, G. C. La Rocca and V. M. Agranovich, *Phys. status solidi*, 2004, **1**, 1429–1438.
- T. Brixner, R. Hildner, J. Köhler, C. Lambert and F. Würthner, *Advanced Energy Materials*, 2017, **7**, 1700236.
- P. Lova, V. Grande, G. Manfredi, M. Patrini, S. Herbst, F. Würthner and D. Comoretto, *Adv. Opt. Mater.*, 2017, **5**, 1700523.
- T. Weil, T. Vosch, J. Hofkens, K. Peneva and K. Müllen, *Angew. Chemie Int. Ed.*, 2010, **49**, 9068–9093.
- F. Würthner, *Chem. Commun.*, 2004, **0**, 1564–1579.
- M. Sun, K. Müllen and M. Yin, *Chem. Soc. Rev.*, 2016, **45**, 1513–1528.
- C. Zhang, T. Liu, W. Zeng, D. Xie, Z. Luo, Y. Sun and C. Yang, *Mater. Chem. Front.*, 2017, **1**, 749–756.
- T. E. Kaiser, H. Wang, V. Stepanenko and F. Würthner, *Angew. Chemie*, 2007, **119**, 5637–5640.
- A. Nowak-Król, K. Shoyama, M. Stolte and F. Würthner, *Chem. Commun.*, 2018, **54**, 13763–13772.
- J. Zhou, W. Zhang, X.-F. Jiang, C. Wang, X. Zhou, B. Xu, L. Liu, Z. Xie and Y. Ma, *J. Phys. Chem. Lett.*, 2018, **9**, 57.
- C. Hippus, F. Schlosser, M. O. Vysotsky, V. Böhmer and F. Würthner, *J. Am. Chem. Soc.*, 2006, **128**, 3870–3871.
- C. W. Struijk and A. B. S. Dakhorst, M. van Dijk, P. Kimkes, R. B. M. Koehorst, H. Donker, T. J. Schaafsma, S. J. Picken, A. M. van de Craats, J. M. Warman, H. Zuilhof, E. J. R. Sudho, *J. Am. Chem. Soc.*, 2000, **122**, 11057–11066.

20. V. Grande, B. Soberats, S. Herbst, V. Stepanenko and F. Würthner, *Chem. Sci.*, 2018, **9**, 6904–6911.
21. Q. Wang, J. L. Mynar, M. Yoshida, E. Lee, M. Lee, K. Okuro, K. Kinbara and T. Aida, *Nature*, 2010, **463**, 339–343.
22. E. Cohen, H. Weissman, E. Shimoni, I. Kaplan-Ashiri, K. Werle, W. Wohlleben and B. Rybtchinski, *Chem. Eur. J.*, 2017, **56**, 2203–2207.
23. F. Würthner, C. R. Saha-Müller, B. Fimmel, S. Ogi, P. Leowanawat and D. Schmidt, *Chem. Rev.*, 2016, **116**, 962–1052.
24. D. Ambrosek, H. Marciniak, S. Lochbrunner, J. Tatchen, X.-Q. Li, F. Würthner and O. Kühn, *Phys. Chem. Chem. Phys.*, 2011, **13**, 17649.
25. F. W. H. Lin, R. Camacho, Y. Tian, T. E. Kaiser, *IG Scheblykin Nano Lett.*, 2010, **2**, 620–626.
26. F. C. Spano and C. Silva, *Annu. Rev. Phys. Chem.*, 2014, **65**, 477–500.
27. S. Ghosh, X. Q. Li, V. Stepanenko and F. Würthner, *Chemistry (Easton)*, 2008, **14**, 11343–11357.
28. W. Wan, L. A. Nafie, D. Korouski, I. K. Lednev, R. K. Dukor, M. Shanmugasundaram, L. Popova, G. Stubbs and X. Lu, *J. Am. Chem. Soc.*, 2014, **136**, 2302–2312.
29. D. Korouski, R. K. Dukor, X. Lu, L. A. Nafie and I. K. Lednev, *Chem. Commun.*, 2012, **48**, 2837–2839.
30. P. Hildebrandt, H. Tamiaki, A. R. Holzwarth and K. Schaffner, *J. Phys. Chem.*, 1994, **98**, 2192–2197.
31. D. McNaughton, S. J. Langford, M. Duriska, J. K. Unthank, B. M. Cooke, F. K. Glenister, J. Lim and B. R. Wood, *J. Am. Chem. Soc.*, 2004, **126**, 9233–9239.
32. B. A. Friesen, C. C. Rich, U. Mazur and J. L. McHale, *J. Phys. Chem. C*, 2010, **114**, 16357–16366.
33. C. C. Rich and J. L. McHale, *J. Phys. Chem. C*, 2013, **117**, 10856–10865.
34. M. Gouterman, *J. Mol. Spectrosc.*, 1961, **6**, 138–163.
35. S. Köhn, H. Kolbe, M. Korgner, C. Köpsel, B. Mayer, H. Auweter, E. Lüddecke, H. Bettermann and H.-D. Martin, in *Carotenoids*, Birkhäuser Basel, 2008, pp. 53–98.
36. E. H. Witlicki, S. W. Hansen, M. Christensen, T. S. Hansen, S. D. Nygaard, J. O. Jeppesen, E. W. Wong, L. Jensen and A. H. Flood, *J. Phys. Chem. A*, 2009, **113**, 9450–9457.
37. M. Suhm, J. P. Simons, W. Caminati, A. Zehnacker, M. A. Suhm, M. Mons, H.-H. Limbach, N. Borho, Y. Xu, J. L. Alonso, *et al.*, *Phys. Chem. Chem. Phys.*, 2007, **9**, 48–94.
38. R. M. Hochstrasser and C. A. Nyi, *J. Chem. Phys.*, 1980, **72**, 2591–2600.
39. M. Angelella, C. Wang and M. J. Tauber, *J Phys Chem A*, 2013, **117**, 9196–9204.
40. M. J. Frisch, G. W. Trucks, H. B. Schlegel, G. E. Scuseria, M. A. Robb, J. R. Cheeseman, G. Scalmani, V. Barone, B. Mennucci, G. A. Petersson, *et al.*, *Gaussian 09*, 2009, pp.
41. E. Runge and E. K. U. Gross, *Phys. Rev. Lett.*, 1984, **52**, 997–1000.
42. R. Bauernschmitt and R. Ahlrichs, *Chem. Phys. Lett.*, 1996, **256**, 454–464.
43. E. F. Pettersen, T. D. Goddard, C. C. Huang, G. S. Couch, D. M. Greenblatt, E. C. Meng and T. E. Ferrin, *J. Comput. Chem.*, 2004, **25**, 1605–1612.
44. R. L. Martin, *J. Chem. Phys.*, 2003, **118**, 4775–4777.
45. T. Lu and F. Chen, *J. Comput. Chem.*, 2012, **33**, 580–592.
46. S. Yamazaki, A. L. Sobolewski and W. Domcke, *Phys. Chem. Chem. Phys.*, 2011, **13**, 1618–1628.
47. A. Toyama, H. Takeuchi and I. Harada, *J. Mol. Struct.*, 1991, **242**, 87–98.
48. G. P. Connolly, Y. Bai, M.-F. Jeng and S. W. Englander, in *PROTEINS Structure, Function, and Genetics*, 1993, pp. **17**, 87–92.
49. S. P. A. Fodor, R. P. Rava, T. R. Hays and T. G. Spiro, *J. Am. Chem. Soc.*, 1985, **107**, 1520–1529.
50. D. L. Akins, *Nanomater. Nanotechnol.*, 2014, **4**, 1.
51. D. M. Coles, A. J. Meijer, W. C. Tsoi, M. D. Charlton, J. S. Kim and D. G. Lidzey, *J Phys Chem A*, 2010, **114**, 11920–11927.
52. Z. Chi, X. G. Chen, J. S. W. Holtz and S. A. Asher, *Biochemistry*, 1998, **37**, 2854–2864.
53. S. A. Asher, A. Ianoul, G. Mix, M. N. Boyden, A. Karnoup, M. Diem and R. Schweitzer-Stenner, *J. Am. Chem. Soc.*, 2001, **123**, 11775–11781.
54. A. Rygula, K. Majzner, K. M. Marzec, A. Kaczor, M. Pilarczyk and M. Baranska, *J. Raman Spectrosc.*, 2013, **44**, 1061–1076.
55. S. Kasiouli, F. Di Stasio, S. O. McDonnell, C. P. Constantinides, H. L. Anderson, F. Cacialli and S. C. Hayes, *J. Phys. Chem. B*, 2013, **117**, 5737–5747.
56. G. Balakrishnan and T. G. Spiro, in *Encyclopedia of Biophysics*, Springer Berlin Heidelberg, 2013, pp. 2697–2707.
57. G. Pieridou, C. Avgousti-Menelaou, P. Tamamis, G. Archontis and S. C. Hayes, *J. Phys. Chem. B*, 2011, **115**, 4088–4098.
58. A. Sarbu, L. Biniek, J.-M. Guenet, P. J. Mésini and M. Brinkmann, *J. Mater. Chem. C*, 2015, **3**, 1235–1242.